Atlantic Multidecadal Variability Response to External Forcing during the Past Two Millennia

ZHANGQI DAI,[a,b] BIN WANG,[c,d] LING ZHU,[a] JIAN LIU,[a,e,f] WEIYI SUN,[a] LONGHUI LI,[a] GUONIAN LÜ,[a] LIANG NING,[a] MI YAN,[a] AND KEFAN CHEN[a]

[a] *Key Laboratory for Virtual Geographic Environment, Ministry of Education, Jiangsu Provincial State Key Laboratory Cultivation Base of Geographical Environment Evolution, Jiangsu Center for Collaborative Innovation in Geographical Information Resource Development and Application, and School of Geography Science, Nanjing Normal University, Nanjing, China*

[b] *Kunshan Lujia Senior High School, Suzhou, China*

[c] *Department of Atmospheric Sciences and Atmosphere–Ocean Research Center, University of Hawai'i at Mānoa, Honolulu, Hawaii*

[d] *Key Laboratory of Meteorological Disaster of Ministry of Education and Earth System Modeling Center, Nanjing University of Information Science and Technology, Nanjing, China*

[e] *Jiangsu Provincial Key Laboratory for Numerical Simulation of Large Scale Complex Systems, School of Mathematical Science, Nanjing Normal University, Nanjing, China*

[f] *Open Studio for the Simulation of Ocean-Climate-Isotope, Qingdao National Laboratory for Marine Science and Technology, Qingdao, China*

(Manuscript received 17 December 2021, in final form 6 August 2022)

ABSTRACT: Atlantic multidecadal variability (AMV) is a cornerstone for decadal prediction and profoundly influences regional and global climate variability, yet its fundamental drivers remain an issue for debate. Studies suggest that external forcing may have affected AMV during the Little Ice Age (AD 1400–1860). However, the detailed mechanism remains elusive, and the AMV's centennial to millennial variations over the past 2000 years have not yet been explored. We first show that proxy-data reconstructions and paleo-data assimilations suggest a significant 60-yr AMV during AD 1250–1860 but not during AD 1–1249. We then conducted a suite of experiments with the Community Earth System Model (CESM) to unravel the causes of the changing AMV property. The simulation results under all external forcings match the reconstructions reasonably well. We find that the significant 60-yr AMV during 1250–1860 arises predominantly from the volcano forcing variability. During the period 1–1249, the average volcanic eruption intensity is about half of the 1250–1860 intensity, and a 20–40-yr internal variability dominates the AMV. The volcanic radiative forcing during 1250–1860 amplifies AMV and shifts the internal variability peak from 20–40 years to 60 years. The volcano forcing prolongs AMV periodicity by sustaining Arctic cooling, delaying subpolar sea ice melting and atmospheric feedback to reduce surface evaporation. These slow-response processes over the subpolar North Atlantic results in a persisting reduction of sea surface salinity, weakening the Atlantic overturning circulation, and warm water transport from the subtropical North Atlantic. The results reveal the cause of the nonstationary AMV over the past two millennia and shed light on the AMV's response to external forcing.

SIGNIFICANCE STATEMENT: AMV plays an important role in the regional and global climate variability. The purpose of this study is to better understand the secular change of AMV during the past 2000 years and its response to the external forcing. Proxy data and model simulation consistently show a significant 60-yr AMV during AD 1250–1860 that is absent during AD 1–1249. Active volcanic eruptions during 1250–1860 amplify the AMV and shift its intrinsic 20–40-yr to a prominent 60-yr variance peak. Volcanoes prolong AMV periodicity by sustaining Arctic cooling, delaying subpolar sea ice melting, reducing evaporation, and increasing surface salinity. These results help us better understand nonstationary AMV and highlight the role of external forcing over the past two millennia.

KEYWORDS: North Atlantic Ocean; Volcanoes; Atmosphere-ocean interaction; Paleoclimate; Multidecadal variability

1. Introduction

Atlantic multidecadal variability (AMV) is a dominant mode of Atlantic SST variability, with a horseshoe-shaped spatial pattern in the North Atlantic (NA) and a 55–90-yr peak in the historical (1850–present) observations (Kushnir 1994; Ting et al. 2009). AMV has profound influences on regional and global climate variability on decadal time scales (Enfield et al. 2001; Ning et al. 2017). It serves as a cornerstone for current decadal prediction. However, the fundamental drivers of AMV remain vigorously debated.

Competing theories and hypotheses have been proposed to explain the AMV's origin, involving internal variability and

Denotes content that is immediately available upon publication as open access.

Supplemental information related to this paper is available at the Journals Online website: https://doi.org/10.1175/JCLI-D-21-0986.s1

Zhangqi Dai and Weiyi Sun contributed equally to the article and should be considered co-first authors.

Corresponding author: Jian Liu, jliu@njnu.edu.cn

DOI: 10.1175/JCLI-D-21-0986.1

external forcing. AMV has been closely related to the Atlantic meridional overturning circulation (AMOC), involving out-of-phase variations in the North and South Atlantic sea surface temperature (SST) (Knight et al. 2005; Delworth et al. 2017). In contrast, Clement et al. (2015) argued that AMV is a low-frequency response to high-frequency atmospheric stochastic forcing. The positive feedback between atmospheric circulation, low-level cloud, and SST may also contribute to the AMV anomalies (Evan et al. 2013). Anthropogenic aerosol was speculated to play an important role in the AMV (Bellomo et al. 2018). Natural external forcing, such as the 11-yr cycle of solar radiation, could influence the NA SST (Thiéblemont et al. 2015; Fang et al. 2021; Klavans et al. 2022; Lapointe and Bradley 2021), causing a negative phase of AMV (Ingleby and Huddleston 2007). Nevertheless, instrumental observations are too short to determine the dominant time scale and identify all possible physical mechanisms leading to AMV.

Analysis of multiple paleo-proxies suggests that AMV extends back several centuries (Gray et al. 2004; Mann et al. 2009; Lapointe et al. 2020). Delworth and Mann (2000) first demonstrated a substantial agreement between the simulated and observed patterns of multidecadal variability in SST over the North Atlantic. Otterå et al. (2010), with a coupled ocean–atmosphere general circulation model, demonstrated that the solar and volcanic forcings largely govern the AMV during the past 600 years. They find volcanoes play a particularly important part in phasing the multidecadal variability through their direct influence on tropical sea surface temperatures, the leading mode of NH atmosphere circulation, and the Atlantic thermohaline circulation.

Proxies and model results have suggested that volcanic eruptions can affect SST and thus have an impact on Atlantic multidecadal variability (Wang et al. 2017; Ning et al. 2017; Sun et al. 2019a,b). The results from the Community Earth System Model (CESM) Last Millennium Ensemble (LME) has shown that the AMV's amplitude increased (Otto-Bliesner et al. 2016; Stevenson et al. 2018), and the AMV index dropped significantly following major volcanic eruptions (Swingedouw et al. 2017; Ning et al. 2017; Lehner et al. 2013; Moreno-Chamarro et al. 2017). Volcanic eruptions may trigger sea ice–ocean feedback in the NA and eventually lead to a sustained cooling on the multidecadal scale as reflected in proxies and models (Miller et al. 2012; Schleussner and Feulner 2013). This feedback is realized through a southward expansion of sea ice that could lead to subpolar Atlantic freshening and stabilization, weakening deep ocean convection (Zhong et al. 2011; Yang and Wen 2020). Recently, Mann et al. (2021) suggested a 50–70-yr cycle of AMV during the past millennium, driven by volcanic eruptions.

The studies mentioned above provide clues for understanding the influence of external forcings on AMV. Nevertheless, previous studies have only focused on the AMV variation over the last millennium. No single volcano or solar forcing sensitivity experiments were conducted to isolate the roles of these external forcing in regulating AMV. The mechanisms by which volcanoes change AMV characteristics remain elusive. In this study, we use the CESM to conduct a suite of 2000-yr experiments to explore the millennial variation of the spatial and temporal characteristics of AMV. The experiments include fixed forcing (control), an all-forcing run, and single-solar and single-volcano forcing simulations. We compare the simulation results with a collection of multiple paleoproxy reconstructions and paleo-assimilation datasets. We aim to reveal long-term changes in the spatial and temporal characteristics of AMV over the past 2000 years and to understand better the critical roles of the external forcing in changing AMV properties. This research particularly investigates the responses of the AMV's periodicity and intensity to volcano forcing and unravels its possible underlying mechanisms.

2. Data and methods

a. *The CESM1 model*

The model used is CESM1 (Hurrell et al. 2013), with a horizontal resolution of T31 (about 3.75° × 3.75°) and a vertical resolution of 26 layers. Previous studies have demonstrated the model's capacity in simulating the influences of volcanic forcing on ENSO, monsoon precipitation, and Arctic climate simulated (Liu et al. 2016; Sun et al. 2019a,b; Liu et al. 2020; Sun et al. 2022). Here we first assessed the performance of CESM in simulating AMV from 1870 to 2000 under the historical external forcing (Fig. S1 in the online supplemental material). The simulated AMV index is significantly correlated with that derived from HadISST (CC = 0.55, $p < 0.05$). The corresponding regressed SST fields in the North Atlantic show similar horseshoe-like patterns with a CC = 0.91, except that the variability center south of Greenland shifted southeastward. The result indicates that the model under the historical external forcing can reproduce, to some extent, the observed AMV, suggesting that the observed AMV might not entirely arise from internal variabilities, and the specified external forcing has a fingerprint on the AMV.

b. *The 2ka simulation and experimental design*

First, a preindustrial experiment with the 1850 background conditions (Rosenbloom et al. 2013) is conducted after a 400-yr spinup when the climate system reaches an energy balance state. A control experiment (Ctrl) runs 2000 years starting from the last year of the spinup run. Three 2000-yr transient climate simulation experiments were carried out starting from the last year of the Ctrl experiment: the solar radiation experiment (TSI), the volcanic activities experiment (Vol), and the all forcing experiment (AF) (Table 1) (Wang et al. 2015; Sun et al. 2017).

We used a relatively large-amplitude solar radiation (Shapiro et al. 2011) to identify its effect on climate better. The volcanic forcing currently used in the Paleoclimate Modeling Intercomparison Project phase 3 (PMIP3) and CESM-LME is the Ice-core Volcanic Index 2 (IVI2) (Gao et al. 2008). The IVI2 contains monthly mean spatiotemporal distributions of volcanic forcing during the past 1500 years. To our knowledge, thus far, no volcanic forcing is available that can be directly used to drive the model during the entire last two millennia. Sigl et al. (2015) reconstructed the volcanic

TABLE 1. Experiments used in this study.

Name	External forcing	Short name	Length of integral time (years)
Control experiment	Preindustrial values (Rosenbloom et al. 2013)	Ctrl	2000
Solar radiation sensitivity experiment	Shapiro et al. (2011)	TSI	2000
Volcanic activity sensitivity experiment	Sigl et al. (2015), Gao et al. (2008)	Vol	2000
All forcing experiment	Shapiro et al. (2011), Sigl et al. (2015), Gao et al. (2008), MacFarling Meure et al. (2006), Kaplan et al. (2011)	AF	2000

activity over the past 2500 years but did not extend it in time and space to directly drive CESM. Therefore, we used the same parameterization method as IVI2 to extend the volcanic activity in time and space for AD 1–500. We then spliced it with IVI2 to generate the volcanic forcing of the past 2000 years.

c. *Observational, reconstructed, and assimilated datasets*

The Hadley Center Sea Ice and Sea Surface Temperature (HadISST) data with a resolution of 1° × 1° (Rayner et al. 2003) are used to verify the model simulation. To facilitate comparison with our simulations, we interpolate the HadISST to the resolution consistent with the experiments (3.75° × 3.75°).

As shown in Table 2, there are three reconstructed AMV records used in this study, which are reconstructed by Gray et al. (2004) (AD 1567–1990), Mann et al. (2009) (AD 500–2006), and Lapointe et al. (2020) (889 BC–AD 2011). Due to the inconsistencies in the lengths of these reconstructed data, to compare with more proxies, we focus on the AMV variation from AD 500 onward. SST reconstructions in the NA (PAGES 2k Consortium 2013) are also considered. There are only six reconstructions that cover the past two millennia (Black et al. 2007; Keigwin et al. 2003; Sachs 2007; Richter et al. 2009; Sicre et al. 2011; Thornalley et al. 2009). This study also uses the annual mean SST derived from the Last Millennium Reanalysis V2.1 (LMR) (Tardif et al. 2019) and the AMV index from the reconstruction of global hydroclimate and dynamical variables (Hydro) (Steiger et al. 2018). These datasets are based on climate model simulations incorporating reconstructed data. For details, the readers are referred to Tardif et al. (2019) and Steiger et al. (2018).

d. *Definition of AMV index*

The AMV index in the simulated results and the LMR is defined as the area-weighted average of the anomaly annual mean SST in the NA (0°–60°N, 7.5°–75°W) (Enfield et al. 2001). The ordinary least squares are used to detrend the AMV index to eliminate the global warming trend and the time trend in the model's output (Trenberth and Shea 2006). In most cases, detrending data highlights their multidecadal variability (Sutton and Hodson 2005).

3. The secular change of AMV during the past 2000 years

Figure 1 compares five reconstructed and two model-simulated AMV indices. The five paleoclimate records show that the AMV index transits from a positive to a negative phase after or during successive large volcanic eruptions, such as the periods 1250–90, 1450–80, 1590–1610, 1630–50, 1755–80, and 1805–40 (light blue shading in Fig. 1). After the active volcanism periods, the AMV rebounds back to a positive phase (light yellow shadings in Fig. 1). The result is consistent with the previous studies (Wang et al. 2017; Otterå et al. 2010). Similar AMV phase transitions are more clearly seen in the CESM AF and Vol simulations (Figs. 1f,g). However, the four proxy records show a moderate cooling after the strongest Samalas eruption in 1258. In contrast, the simulated AMV shows an abrupt large-amplitude cooling, indicating a considerable disparity between the model and proxy data, and across proxy data themselves. For example, the Hydro and Lapointe et al. (2020) time series are rather flat; Mann

TABLE 2. Reconstruction and assimilation data used in this study.

Type	Location	Climate indicators	Period	Reference
Tree ring	0°–70°N, 100°W–40°E	AMV	AD 1567–1990	Gray et al. (2004)
Multiple proxies	North Atlantic	AMV	AD 500–2006	Mann et al. (2009)
Lake sediment core	Ellesmere Island	AMV	889 BC–AD 2011	Lapointe et al. (2020)
Mg/Ca ratio	10.77°N, 64.77°W	SST	AD 1221–1990	Black et al. (2007)
UK37	45.89°N, 62.8°W	SST	AD 351–1950	Keigwin et al. (2003)
UK37	43.53°N, 62.48°W	SST	AD 400–1950	Sachs (2007)
Mg/Ca ratio	55.5°N, 13.9°W	SST	AD 1–1998	Richter et al. (2009)
^{14}C	66.55°N, 17.42°W	SST	AD 2–2001	Sicre et al. (2011)
Mg/Ca ratio	62.08°N, 17.82°W	SST	AD 33–1950	Thornalley et al. (2009)
Assimilation (LMR)	North Atlantic	AMV	AD 1–2000	Tardif et al. (2019)
Assimilation (Hydro)	North Atlantic	AMV	AD 1–2000	Steiger et al. (2018)

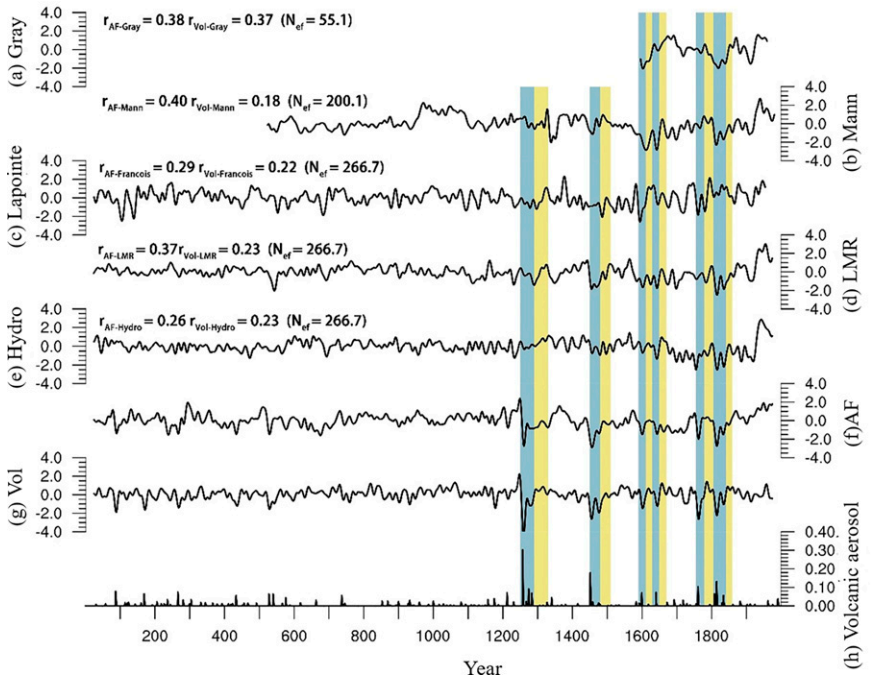

FIG. 1. The simulated and reconstructed AMV index during the past 2000 years. (a)–(c) The AMV index reconstructed by Gray et al. (2004), Mann et al. (2009), and Lapointe et al. (2020). (d),(e) The AMV index in the LMR and Hydro and (f),(g) the AMV index in the AF and Vol experiments. (h) The volcanic forcing. The upper-left numbers in (a)–(e) are the correlation coefficients between reconstructions and AF and Vol experiments, and the numbers in parentheses are the effective degrees of freedom. The periods of intense volcanic activity are marked by the light blue shading, while the periods of weak volcanic activity after the active volcanoes are marked by the light yellow shading. All data are 15-yr low-pass filtered before analysis.

et al. (2009) cools much later; and the LMR cooling is not as strong as in the models.

The Samalas eruption was the most prominent volcano during the past 2000 years, followed by many powerful volcanic eruptions (Fig. 1h) (Gao et al. 2008; Sigl et al. 2015). It could have triggered the first cooling phase of the Little Ice Age (Miller et al. 2012; Slawinska and Robock 2018). The average intensity of volcanic eruptions is 15.2 Tg during 500–1249, but increased to 30.6 Tg during 1250–1860, more than doubled. Thus, we will focus on two periods, 500–1249 and 1250–1860, to investigate the response of AMV to the different volcanic forcing on the multidecadal time scale.

Figure 2 compares the reconstructed and simulated spectra of the AMV index during two contrasting volcano forcing periods: 500–1249 and 1250–1860. During 500–1249, the spectrum peaks in the reconstructions and assimilations vary considerably. The reconstructions show a salient 95-yr peak (Figs. 2a,c) while the LMR shows a double peak at 55 and 80–85 years, respectively (Fig. 2e), and Hydro shows significant 20–35-yr and 50–60-yr peaks (Fig. 2g). The inconsistency among proxy datasets suggests a considerable uncertainty in the proxy data. The AF and Vol experiments display marginally significant peaks at 30–40 and 80–85 years (Figs. 2i,m). On the other hand, the Ctrl (fixed forcing) experiment exhibits a prominent 20–35-yr peak and a marginal 95-yr peak (Fig. 2o). To some extent, the forced (AF and Vol) and unforced (Ctrl) runs have similar power spectra, suggesting that the external forcings did not substantially alter the periodicity of the intrinsic AMV during 500–1249.

In contrast, during 1250–1860, a conspicuous 60-yr peak is found across all presented paleo-datasets, including the two reconstructions and two assimilations (LMR and Hydro) (Figs. 2b,d,f,h). In the AF run, a 60-yr-cycle is significant (Fig. 2j), resembling the reconstruction and assimilation. Analysis of each single-forcing run indicates that the Vol run exhibits a significant 60-yr peak (Fig. 2n), whereas the TSI experiment has no significant multidecadal peak (Fig. 2l). Since the Ctrl run has no significant 60-yr peak (Fig. 2o), the significant 60-yr peak of AMV does not arise from the internal variability. It must be shaped by the volcanic forcing during 1250–1860. We also explore the results from five volcanic experiments of the CESM-LME and find that four of them show a 60-yr peak (Fig. S2), supporting our result from an ensemble simulation. We further analyzed the two volcanic reconstruction results, as shown in Fig. S3. Different volcanic reconstructions showed significant 60-yr cycles between 1250 and 1860, further suggesting that this cycle was influenced by volcano activity.

Wavelet analysis of the temporal variation of the spectra reveals a sudden change of periodicity and intensity around

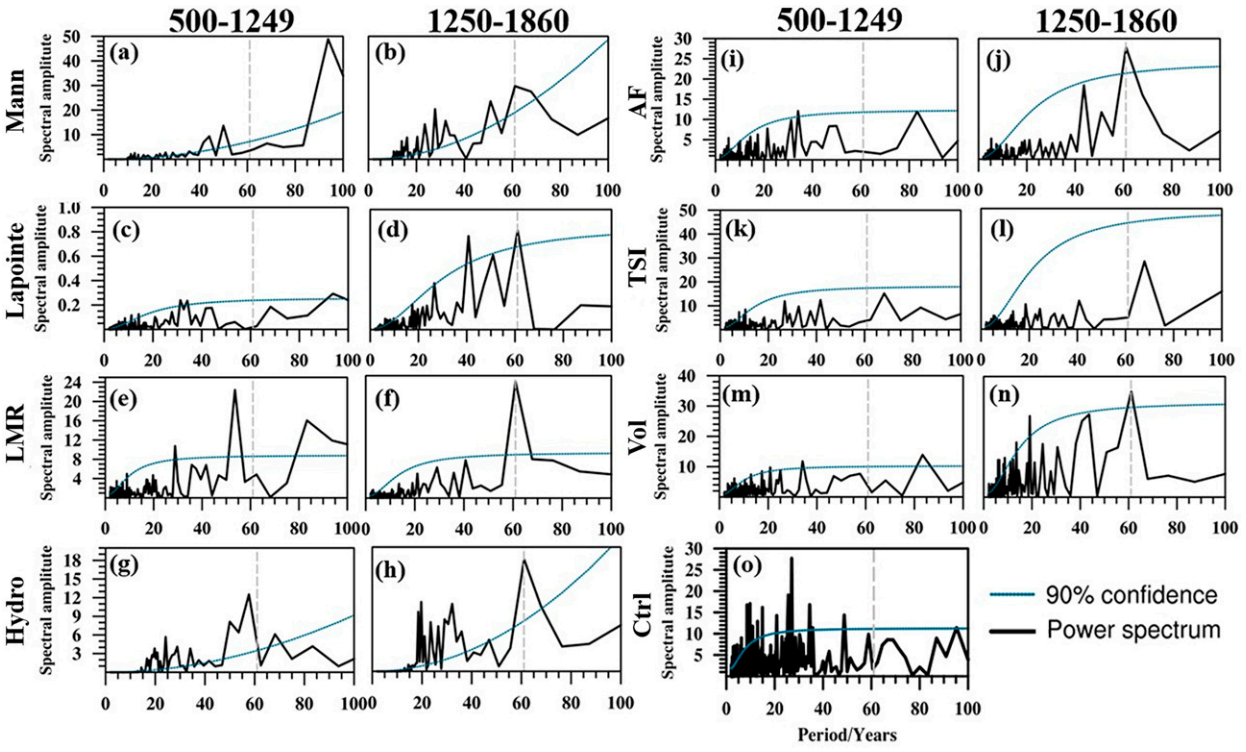

FIG. 2. The power spectrum analysis of AMV derived from the reconstructed, assimilated, and simulated data during 500–1249 and 1250–1860. (left) The reconstructed AMV by (a),(b) Mann et al. (2009) and (c),(d) Lapointe et al. (2020) and (right) the assimilated AMV by (e),(f) LMR and (g),(h) Hydro. (right) The (i),(j) AF experiment, (k),(l) TSI experiment, (m),(n) Vol experiment, and (o) Ctrl experiment. The black line is the power spectrum, and the blue line represents 90% confidence. The dashed lines mark the significant 60-yr cycle.

1250 across all four proxy datasets and the model-forced (AF and Vol) simulations (Fig. 3). This result indicates that during 500–1249, the AMV is weak and lacks a coherent periodicity. In contrast, during 1250–1860, the AMV variance sharply increased, and a prominent 60-yr periodicity emerged. Interestingly, proxy datasets of the wavelet spectrum are consistent with that of the Vol run (Fig. 3f), suggesting an intrinsic linkage between the secular evolution of AMV property and the volcano eruptions. At the same time, we should also pay attention to this point that the patterns are clearly different across the reconstructions, even when they are supposed to reflect the same AMV. For example, the LMR has an energy maximum around 1500 that is absent in Mann et al. (2009) and Lapointe et al. (2020). The Hydro, by contrast, has very little energy at the 60-yr variance level before 1700. There are also interesting differences between AF and Vol that are barely discussed by the authors. Vol has most of the energy around the Samalas and the Tambora eruptions (including the 60-yr variance), smaller amounts around the 1400 and 1600 Huaynaputina eruptions between the 20- and 40-yr variance, and very little energy at longer time scales in between. By contrast, AF has energy more evenly distributed between the two biggest eruptions at the 60-yr variance level. This might reflect a role of other forcing in driving AMV variability.

Figure 4 presents spatial variations of the SST anomalies associated with the significant 60-yr AMV during 1250–1860. We derived the internal mode of AMV from the control experiment with a 15–39-yr bandpass filtered data and the volcano-forced mode from the Vol experiment with a 45–81-yr bandpass filtered data. Both the internal mode and volcano-forced mode display significant cooling centered the south of Greenland and Iceland. However, the cooling amplitude in the volcano-forced mode is stronger than that in the internal mode. To confirm that the regression pattern (Fig. 4b) is mainly affected by the volcanic eruptions, we made composite SST changes between the periods of successive volcanic eruptions and the following weak volcanoes (light blue minus yellow shadings in Fig. 1) in the LMR and Vol experiment (Figs. 4c,d). The spatial pattern in the regression analysis resembles that in the composite analysis (Figs. 4b,d), with a pattern correlation coefficient of 0.71 ($p < 0.01$). The result in Fig. 4 suggests that the successive strong volcanic eruptions-induced cooling might contribute to the cooling phase of the significant 60-yr oscillation in the Vol experiment.

The cooling centers in the volcano-forced mode (Figs. 4b,d) seem to resemble the center of the internal mode (Fig. 4a), suggesting a signature of the model's internal variability in the forced mode, or the forced mode might be modulated from the internal mode. Furthermore, both reconstruction (Figs. 1a–e) and simulation (Figs. 1f,g) show the AMV amplified after 1250.

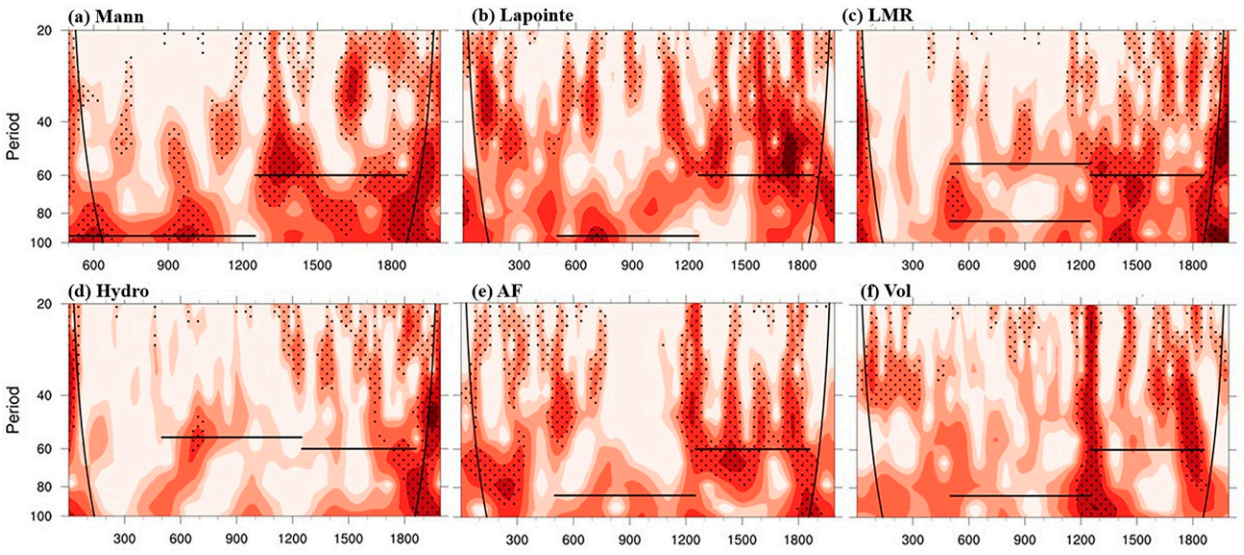

FIG. 3. The wavelet analysis of AMV derived from the reconstructed, assimilated, and simulated data after 9 years of low-pass filtering. The black lines represent significant peaks during 500–1249 and 1250–1860 as measured by power spectrum analysis. Mann reconstructed the data from the year 500 so it only shows the data from 500 to 2000. The black dots indicate that the results are significant at the 90% confidence level.

4. The mechanism of volcanic eruption driving AMV during 1250–1860

The evidence shown in the previous section suggests that volcanic eruption may induce a negative phase of AMV. But how do volcanoes excite the negative phase of AMV? How could volcano forcing set up a 60-yr variance peak that is longer than the internal AMV mode?

There are several possibilities for volcanoes affecting AMV. First, the decrease in solar radiation may cool the Atlantic SST. However, it is unclear whether this alone can account for the cooling pattern (Ineson et al. 2011). Second, the global cooling pattern in response to volcanic forcing has the largest variance in the tropical oceans (Otto-Bliesner et al. 2016). The Gulf Stream and North Atlantic drift may further affect the extratropical and subpolar NA SST (Mann et al. 2021). However, the largest cooling center in the significant 60-yr variations is in the subpolar NA, not in the tropics. The third possibility, and more likely, is that the volcanic eruption has the longest-lasting effect on Arctic sea ice (Liu et al. 2020). Thus, the sea ice expansion could affect the NA (Slawinska and Robock 2018). Previous studies have suggested the sea ice–albedo feedback in expanding the Arctic sea ice extent and reducing the surface temperature over the polar and subpolar regions (e.g., Slawinska and Robock 2018;

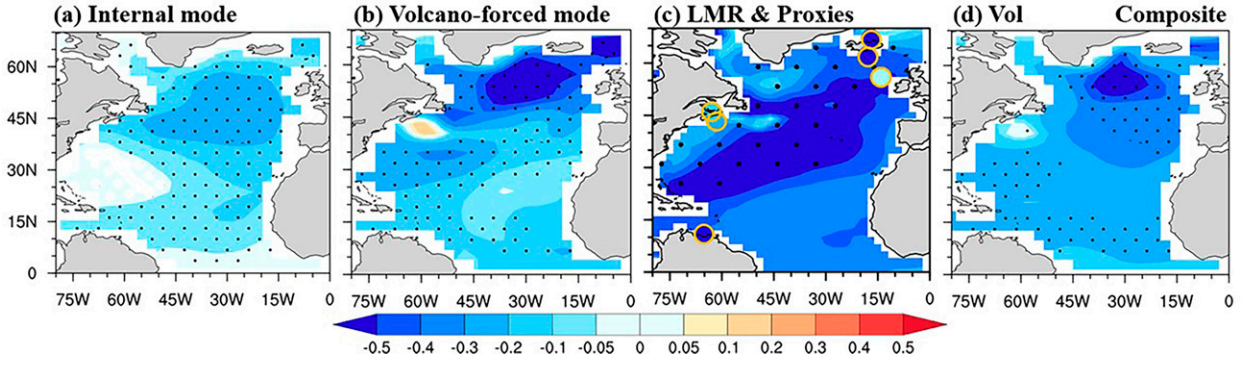

FIG. 4. The linkage between the SST and AMV during 1250–1860. Bandpass filtering is performed for 15–39 years in the Ctrl experiment and 45–81 years in the Vol experiment to extract the internal mode and volcano-forced mode, respectively. (a),(b) The AMV and SST regression results (units: °C) in the Ctrl and Vol experiments. (c),(d) The composite of SST difference between the active volcanic eruptions periods (1250–90, 1450–80, 1590–1610, 1630–50, 1755–80, and 1805–40) and the periods after the eruptions (1290–1330, 1480–1510, 1610–30, 1650–70, 1780–1805, and 1840–60) in LMR and Vol experiment from 1250 to 1860, where (c) is the standardized result and the unit of (d) is °C. The six yellow-framed dots in (c) are reconstruction data. The black dots indicate that the results are significant at the 90% confidence level.

Robock 2000). Ménégoz et al. (2018) found a southward expansion of sea ice after the volcanic eruption resulted in a stronger cooling in the 40°–60°N region of the AMV.

We find close associations between the forced AMV and a chain reaction of the Arctic sea ice area, downward shortwave radiation, and albedo averaged over the subpolar (45°–65°N, 0°–60°W) NA during the past 2000 years (Fig. S4a). All of these quantities have been bandpass filtered for 45–81 years. During 1250–1960 the AMV index is significantly correlated to the sea ice area ($r = -0.79$, $p < 0.01$), shortwave radiation ($r = 0.67$, $p < 0.01$), and albedo (-0.86). These correlations are more significant than any 610-yr period between 1 and 1249 (Fig. S4b). This provides evidence that the volcanic activity on the multidecadal time scale influences the AMV through expanding Arctic cooling by the positive sea ice–albedo feedback.

As noted earlier, the sea ice in the subpolar NA may be expanded in response to volcanic eruptions (Ménégoz et al. 2018). The increased sea ice cover reduces ocean heat loss to the atmosphere, providing a positive surface buoyancy flux and thus disfavoring oceanic convection (Zhong et al. 2011). The observations also show the mass transfer of low-salinity water from the Arctic to the subpolar Atlantic (the so-called Great Salinity Anomaly) cooled the NA during 1968–82 (Dickson et al. 1988; Wang et al. 2021). Increased sea ice and freshwater export from the Arctic has also been proposed to drive LIA cooling by weakening the subpolar gyre (Moreno-Chamarro et al. 2017). Is the expansion of the sea ice area synchronized with changes in SSS?

To facilitate comparison of the internal and volcano-forced mode and to illuminate the role of the SSS anomaly in sustaining NA cooling, we calculate the lead–lag correlation of the sea ice extent, sea ice melt, SSS, and oceanic upwelling with respect to AMV over the polar and subpolar North Atlantic (45°–65°N, 0°–60°W). We note that for the volcano-forced mode, the Arctic sea ice extent lags AMV by 2 years. The subsequent sea ice melt further lags AMV by 4 years. The resultant SSS lags by 5–6 years, and the oceanic upwelling lags by 7 years (Fig. 5b). For the internal mode, the corresponding lags are 0.5–1 year (Fig. 5a). Thus, these low SST anomalies have been sustained for a longer period by the melting ice in the volcano-forced run. Therefore, we suggest that the melting of sea ice 2 years after the sea ice area expansion could inject freshwater into the ocean, further reducing SSS and sustaining desalination and NA cooling. This has implications for the prolonged AMV periodicity.

In terms of spatial distribution, the sea ice expansion reaches as far south as 45°N under volcanism (Fig. 5d). The intensity is stronger than that in the internal mode. Compared with the internal mode (Fig. 5e), the sea ice melting area in the volcano-forced mode extended farther south. As a result, the SSS to the southeastern tip of Greenland decreases significantly (Fig. 5h), similar to the Great Salinity Anomaly (Dickson et al. 1988). Colder water in the subpolar NA upwells to the mixed layer (Fig. 5j), reducing the sinking of seawater and leading to a sustained and significant SST decrease.

Moreover, the surface temperature drops more dramatically under the volcanism than in the internal mode (Figs. 6c,d), and two high pressure centers in the Labrador Sea and the northeast Atlantic occur (Fig. 6f), generating the anticyclone anomalies. Under the control of these anticyclone anomalies, the anomalous 1000-hPa easterlies between 45° and 60°N weaken the mean westerlies. The reduced wind speed and the decreased temperature contribute to reducing the latent heat flux from the ocean to the atmosphere (Fig. 6h). The latent heat flux lags behind AMV by about 5 years in the volcano-forced mode (Fig. 6b). The decreased evaporation further reduces the SSS, weakening the seawater subsidence in the subpolar region and slowing down the northward transport of warm water from the subtropical NA (not shown). We checked the composite of sea ice extent, sea ice melting, sea surface salinity, ocean upwelling, sea level pressure, and 1000-hPa wind before and after several major volcanic eruption events (Fig. S5). We found that the results of the composite were very consistent with the regression results.

On the horizontal energy transports, we examined the oceanic northward heat transport during 1250–1860 from control and the volcano experiments (Fig. 7). We find that the northward heat transport from the ocean in the North Atlantic decreases more significantly in the volcanic mode, compared with Ctrl run, helping to keep the North Atlantic cooling.

5. Summary and discussion

We explored the long-term changes of the AMV's properties over the past 2000 years. The proxy-data reconstructions and paleo-data assimilations suggest a significant 60-yr AMV during 1250–1860 but not during 1–1249 (Fig. 2). The simulation results with CESM under all external forcing match the reconstructions reasonably well. Numerical experiment results suggest that during 1–1249 under relatively inactive volcanos, the AMV is dominated by a 20–40-yr internal variability. The active volcanic radiative forcing during 1250–1860 amplified AMV and shifted the internal variability peak from 20–40 years to about 60 years (Figs. 3 and 4).

We elucidated the mechanism of this significant 60-yr AMV response to the volcanic eruptions by comparing the behavior of the volcano-forced and internal modes. During 1250–1860, the influence of volcanic activity on AMV cycle showed two aspects. The first is to prolong the AMV cycle itself. Under volcanism, the AMV cycle was extended from 20–40 to 60 years. The second is the modulation of volcanoes on the AMV cycle. The volcanic forcing itself has a 60-yr oscillation. Under the influence of this 60-yr oscillation, the internal oscillation cycle of AMV is close to 60 years. We propose that the processes by which volcanoes modulate AMV involve a fast and a slow response (Fig. 8). The fast-response stage is caused by the sea ice expansion, while the freshwater in the subpolar NA dominates the slow-response stage. Arctic sea ice rapidly increases in the fast-response stage and expands to the subpolar NA due to the sea ice–albedo feedback, cooling SST. The initial oceanic surface cooling is due to reduced incoming solar radiation, dimmed by volcanic aerosols. This process has been pointed out in

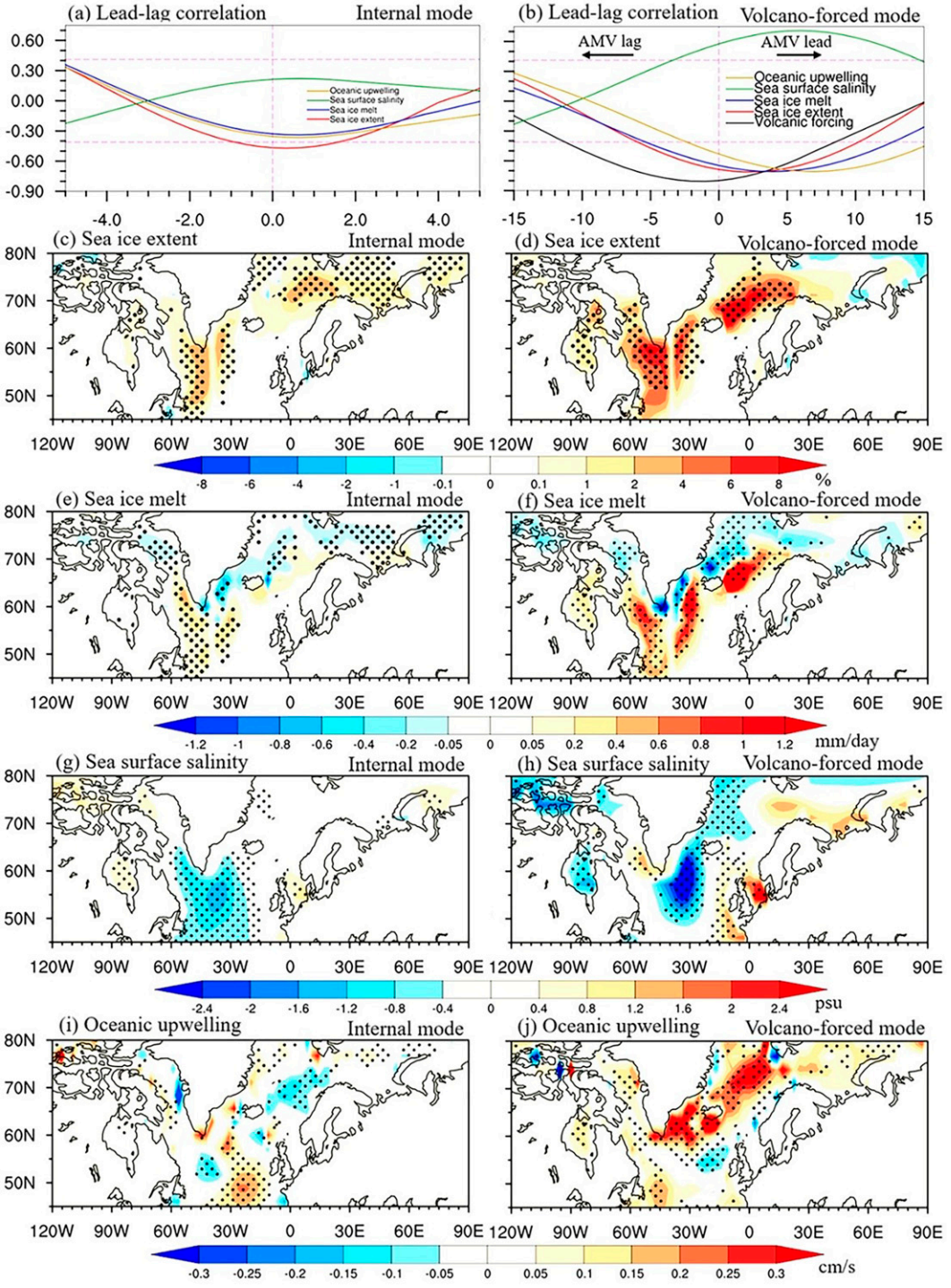

FIG. 5. (a),(b) The lead–lag correlation between sea ice extent (red line), sea ice melt (blue line), SSS (green line), oceanic upwelling (yellow line), and AMV over the polar and subpolar regions of the North Atlantic (45°–65°N, 0°–60°W). (c),(d) Annual mean sea ice extent (units: %), (e),(f) sea ice melt (units: mm day^{-1}), (g),(h) sea surface salinity (units: psu), and (i),(j) 0–100-m average oceanic upwelling (units: cm s^{-1}) regressed with the AMV (left) in Ctrl and (right) during 1250–1860 in the Vol experiments. The black line in (b) is the lead–lag correlation between AMV and the global volcanic sequence. The purple dotted line represents a significance level of 0.1. Bandpass filtering is performed for 15–39 years in the Ctrl experiment and 45–81 years in the Vol experiment to extract the internal mode and volcano-forced mode, respectively. The black dots indicate that the results are significant at the 90% confidence level.

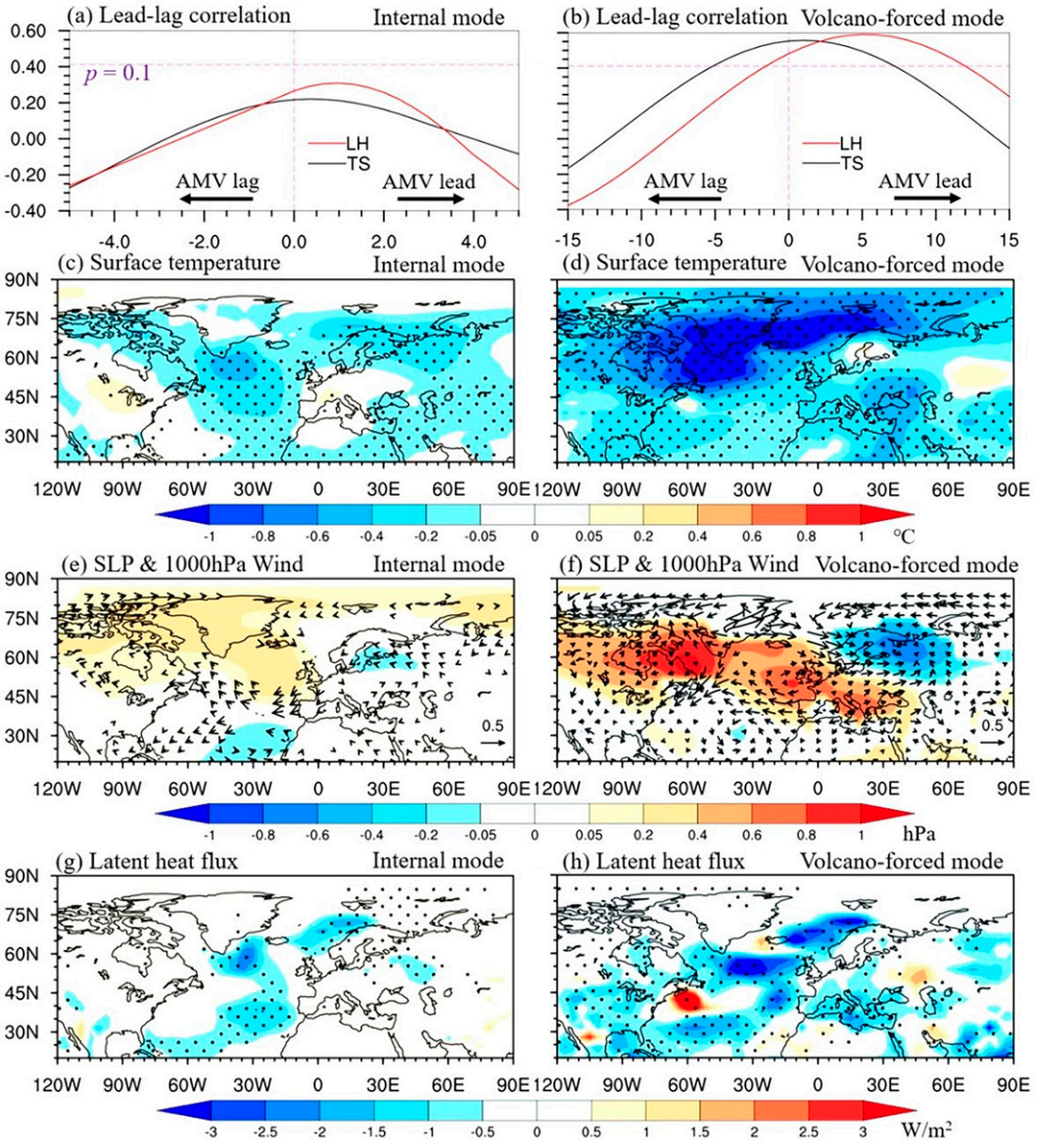

FIG. 6. (a),(b) The lead–lag correlation between surface temperature (black line), latent heat flux (red line), and AMV over the polar and subpolar regions of North Atlantic (45°–65°N, 0°–60°W) after the application of (left) a 15–39-yr bandpass filter in the Ctrl experiment and (right) a 45–81-yr bandpass filter in the Vol experiments. Also shown are annual mean (c),(d) surface temperature (units: °C), (e),(f) sea level pressure (unit: hPa) and 1000-hPa wind (unit: m s^{-1}) and (g),(h) latent heat (unit: W m^{-2}) regressed with the AMV (left) in Ctrl and (right) during 1250–1860 in the Vol experiments after the application of a 45–81-yr bandpass filter. The purple dotted line in (a) and (b) represents a significance level of 0.1. Note that (e) and (f) only draw the wind fields that pass the 90% significance test. The black dots indicate that the results are significant at the 90% confidence level.

previous studies (e.g., Zhong et al. 2011). We find the slow-response stage plays a critical role in the AMV's response to volcano forcing. In the slow-response stage, the expanded sea ice (lag AMV 2 years) melts locally (lag AMV 4 years), injecting freshwater into the ocean and decreasing SSS (lag AMV 5–6 years), thus suppressing ocean convection (lag AMV 7 years) and allowing more cold water to stay on the surface. At the same time, the NA surface wind speed reduces, suppressing evaporation (lag AMV 5 years) and trapping more freshwater in the ocean. The weakening ocean convection during the slow-response stage prolongs NA cooling, extending the intrinsic AMV period and setting up the 60-yr periodicity for the volcano-forced mode. The slow-response stage may explain the prolonged NA cooling after a major volcano eruption shown in proxy data (Fig. 1).

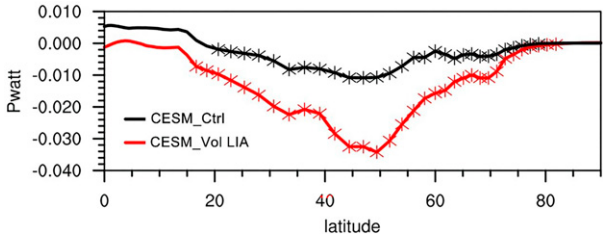

FIG. 7. The northward heat transport in the North Atlantic regressed with the AMV in Ctrl (black) and during 1250–1860 in Vol experiments (red). An asterisk indicates that a significance test of 0.01 has been passed.

The results here enlighten the cause of the nonstationary behavior of AMV over the past two millennia and the processes by which AMV responds to volcano forcing. The anthropogenic forcing affects Arctic temperature change drastically through the ice-albedo feedback, but in an opposite direction as the volcano forcing.

A recent study suggested that the AMV periodicity is linked to the buoyancy frequency and Rossby wave speed (Cheng et al. 2016). We reexamined buoyancy frequencies and Rossby wave speed but found no significant changes under the volcano forcing (Fig. S6). We hypothesize that both the sea ice melting and evaporation's weakening directly led to the SSS decline, weakening the seawater subsidence. We checked the NAO and AMOC from the volcano experiment from 1250 to 1860. Neither AMOC nor NAO had a 60-yr cycle (figure not shown). So, at this time, NAO and AMOC do not seem to have an effect on the 60-yr cycle.

Like any climate data, paleoclimatic reconstructions have their advantages and disadvantages. Climate reconstruction data can extend our knowledge of Earth's climate system beyond the record of instrumental measurements. However, paleoclimate records are often limited by temporal and spatial resolution. The uncertainty of the reconstructed data comes from source limitation, including the temporal resolution, dating error, climate meaning, and indicated seasons. The data we selected all indicated AMV. However, some of these data are characterized by strong correlations between SST in the North Atlantic and other climate variables, as reconstructed by Lapointe et al. (2020). They have no direct response to sea surface temperatures throughout the North Atlantic. The stability of this correlation is still controversial, arguing that a single point record representing climate change in a region needs to be further verified. In terms of time resolution, most of the data we selected are annual resolutions, but there is a 5–10-yr dating error (Lapointe et al. 2020; Mann et al. 2009). In terms of the climatic significance of reconstructed records, the tree rings used in the reconstruction of LMR and Mann et al. (2009) are often considered to reflect the temperature changes of the growing season and the average summer temperature. Our definition of AMV uses an average annual SST, so there may be some uncertainty.

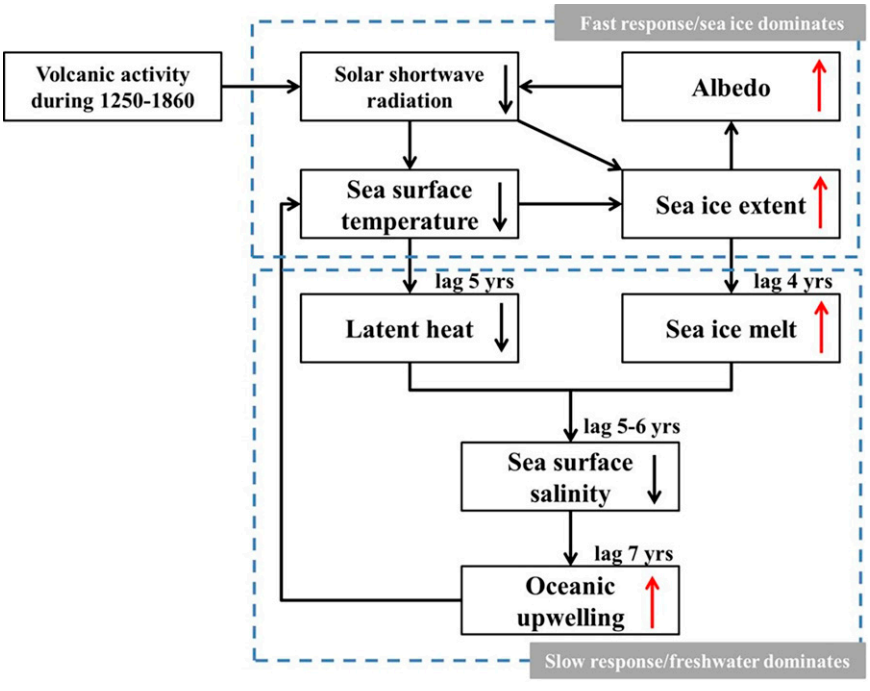

FIG. 8. The possible mechanism of AMV significant 60-yr cycle under volcanism. The upward (downward) arrows represent increase (decrease) of a quantity. The fast response is a synchronous positive feedback caused by sea ice anomaly. The slow-response stage is the delayed feedback caused by freshwater anomaly. Lag refers to years that lag behind AMV.

The model's biases might influence the results. The pattern in the AF experiment shows the maximum SST anomaly shifting farther east than observed (Fig. S1), although the variability center in the Ctrl experiment (Fig. 4a) resembles the observation. This shift is also reflected in the PMIP3 models (Ruiz-Barradas et al. 2013; Kavvada et al. 2013). CESM tends to overestimate climatological sea ice extent for all months, associated with strong westerly winds (Landrum et al. 2012; Ma et al. 2020). Thus, CESM might overestimate the response of the sea ice to volcanoes. Due to the complex mechanism of AMV, more sensitivity experiments and multimodel studies are needed in future studies.

Acknowledgments. We thank the paleoclimate researchers who provided the proxy records (shown in Table 2) and the NOAA and the Hadley Center datasets. We also acknowledge PMIP and CESM-LME for providing the climate simulation data. This research is jointly supported by the National Natural Science Foundation of China (42130604, 41971108, 42105044, 42111530182, and 91437218), and the Program of Innovative Research Team of Jiangsu Higher Education Institutions of China, Priority Academic Program Development of Jiangsu Higher Education Institutions (164320H116).

Data availability statement. The 2ka experiments used during this study in Table 1 are openly available from the Yangtze River Delta Science Data Center, National Earth System Science Data Sharing Infrastructure, National Science and Technology Infrastructure of China (http://dky.njnu.edu.cn). The reconstruction and assimilation data used in Table 2 are available from NOAA's National Centers for Environmental Information (https://www.ncdc.noaa.gov/).

REFERENCES

Bellomo, K., L. N. Murphy, M. A. Cane, A. C. Clement, and L. M. Polvani, 2018: Historical forcings as main drivers of the Atlantic multidecadal variability in the CESM large ensemble. *Climate Dyn.*, **50**, 3687–3698, https://doi.org/10.1007/s00382-017-3834-3.

Black, D. E., M. A. Abahazi, R. C. Thunell, A. Kaplan, E. J. Tappa, and L. C. Peterson, 2007: An 8-century tropical Atlantic SST record from the Cariaco basin: Baseline variability, twentieth-century warming, and Atlantic hurricane frequency. *Paleoceanogr. Paleoclimatol.*, **22**, PA4204, https://doi.org/10.1029/2007PA001427.

Cheng, J., Z. Liu, S. Zhang, W. Liu, L. Dong, P. Liu, and H. Li, 2016: Reduced interdecadal variability of Atlantic meridional overturning circulation under global warming. *Proc. Natl. Acad. Sci. USA*, **113**, 3175–3178, https://doi.org/10.1073/pnas.1519827113.

Clement, A., K. Bellomo, L. N. Murphy, M. A. Cane, T. Mauritsen, G. Radel, and B. Stevens, 2015: The Atlantic multidecadal oscillation without a role for ocean circulation. *Science*, **350**, 320–324, https://doi.org/10.1126/science.aab3980.

Delworth, T. L., and M. E. Mann, 2000: Observed and simulated multi-decadal variability in the Northern Hemisphere. *Climate Dyn.*, **16**, 661–676, https://doi.org/10.1007/s003820000075.

——, F. Zeng, L. Zhang, R. Zhang, G. A. Vecchi, and X. Yang, 2017: The central role of ocean dynamics in connecting the North Atlantic Oscillation to the extratropical component of the Atlantic multidecadal oscillation. *J. Climate*, **30**, 3789–3805, https://doi.org/10.1175/JCLI-D-16-0358.1.

Dickson, R. R., J. Meincke, S.-A. Malmberg, and A. J. Lee, 1988: The "great salinity anomaly" in the northern North Atlantic 1968–1982. *Prog. Oceanogr.*, **20**, 103–151, https://doi.org/10.1016/0079-6611(88)90049-3.

Enfield, D. B., A. M. Mestas-Nuñez, and P. J. Trimble, 2001: The Atlantic multidecadal oscillation and its relation to rainfall and river flows in the continental U.S. *Geophys. Res. Lett.*, **28**, 2077–2080, https://doi.org/10.1029/2000GL012745.

Evan, A. T., R. J. Allen, R. Bennartz, and D. J. Vimont, 2013: The modification of sea surface temperature anomaly linear damping time scales by stratocumulus clouds. *J. Climate*, **26**, 3619–3630, https://doi.org/10.1175/JCLI-D-12-00370.1.

Fang, S. W., M. Khodri, C. Timmreck, D. Zanchettin, and J. Jungclaus, 2021: Disentangling internal and external contributions to Atlantic multidecadal variability over the past millennium. *Geophys. Res. Lett.*, **48**, e2021GL095990, https://doi.org/10.1029/2021GL095990.

Gao, C., A. Robock, and C. Ammann, 2008: Volcanic forcing of climate over the past 1500 years: An improved ice core-based index for climate models. *J. Geophys. Res.*, **113**, D23111, https://doi.org/10.1029/2008JD010239.

Gray, S. T., L. J. Graumlich, J. L. Betancourt, and G. T. Pederson, 2004: A tree-ring based reconstruction of the Atlantic multidecadal oscillation since 1567 A.D. *Geophys. Res. Lett.*, **31**, L12205, https://doi.org/10.1029/2004GL019932.

Hurrell, J. W., and Coauthors, 2013: The Community Earth System Model: A framework for collaborative research. *Bull. Amer. Meteor. Soc.*, **94**, 1339–1360, https://doi.org/10.1175/BAMS-D-12-00121.1.

Ineson, S., A. A. Scaife, J. R. Knight, J. C. Manners, N. J. Dunstone, L. J. Gray, and J. D. Haigh, 2011: Solar forcing of winter climate variability in the Northern Hemisphere. *Nat. Geosci.*, **4**, 753–757, https://doi.org/10.1038/ngeo1282.

Ingleby, B., and M. Huddleston, 2007: Quality control of ocean temperature and salinity profiles historical and real-time data. *J. Mar. Syst.*, **65**, 158–175, https://doi.org/10.1016/j.jmarsys.2005.11.019.

Kaplan, J. O., K. M. Krumhardt, E. C. Ellis, W. F. Ruddiman, C. Lemmen, and K. K. Goldewijk, 2011: Holocene carbon emissions as a result of anthropogenic land cover change. *Holocene*, **21**, 775–791, https://doi.org/10.1177/0959683610386983.

Kavvada, A., A. Ruiz-Barradas, and S. Nigam, 2013: AMO's structure and climate footprint in observations and IPCC AR5 climate simulations. *Climate Dyn.*, **41**, 1345–1364, https://doi.org/10.1007/s00382-013-1712-1.

Keigwin, L. D., J. P. Sachs, and Y. Rosenthal, 2003: A 1600-year history of the Labrador Current off Nova Scotia. *Climate Dyn.*, **21**, 53–62, https://doi.org/10.1007/s00382-003-0316-6.

Klavans, J. M., A. C. Clement, M. A. Cane, and L. N. Murphy, 2022: The evolving role of external forcing in North Atlantic SST variability over the last millennium. *J. Climate*, **35**, 2741–2754, https://doi.org/10.1175/JCLI-D-21-0338.1.

Knight, J. R., R. J. Allan, C. K. Folland, M. Vellinga, and M. E. Mann, 2005: A signature of persistent natural thermohaline circulation cycles in observed climate. *Geophys. Res. Lett.*, **32**, L20708, https://doi.org/10.1029/2005GL024233.

Kushnir, Y., 1994: Interdecadal variations in North Atlantic sea surface temperature and associated atmospheric conditions.

J. Climate, **7**, 141–157, https://doi.org/10.1175/1520-0442(1994)007<0141:IVINAS>2.0.CO;2.

Landrum, L., M. M. Holland, D. P. Schneider, and E. Hunke, 2012: Antarctic sea ice climatology, variability, and late twentieth-century change in CCSM4. *J. Climate*, **25**, 4817–4838, https://doi.org/10.1175/JCLI-D-11-00289.1.

Lapointe, F., and R. S. Bradley, 2021: Little Ice Age abruptly triggered by intrusion of Atlantic waters into the Nordic seas. *Sci. Adv.*, **7**, eabi8230, https://doi.org/10.1126/sciadv.abi8230.

——, and Coauthors, 2020: Annually resolved Atlantic sea surface temperature variability over the past 2,900 y. *Proc. Natl. Acad. Sci. USA*, **117**, 27171–27178, https://doi.org/10.1073/pnas.2014166117.

Lehner, F., A. Born, C. C. Raible, and T. F. Stocker, 2013: Amplified inception of European Little Ice Age by sea ice–ocean–atmosphere feedbacks. *J. Climate*, **26**, 7586–7602, https://doi.org/10.1175/JCLI-D-12-00690.1.

Liu, B., B. Wang, J. Liu, D. Chen, L. Ning, M. Yan, W. Sun and K. Chen, 2020: Global and polar region temperature change induced by single mega volcanic eruption based on Community Earth System Model simulation. *Geophys. Res. Lett.*, **47**, e2020GL089416, https://doi.org/10.1029/2020GL089416.

Liu, F., J. Chai, B. Wang, J. Liu, X. Zhang, and Z. Wang, 2016: Global monsoon precipitation responses to large volcanic eruptions. *Sci. Rep.*, **6**, 24331, https://doi.org/10.1038/srep24331.

Ma, J., S. Xu, and B. Wang, 2020: Reducing numerical diffusion in dynamical coupling between atmosphere and ocean in Community Earth System Model version 1.2.1. *J. Adv. Model. Earth Syst.*, **12**, e2020MS002052, https://doi.org/10.1029/2020MS002052.

MacFarling Meure, C., D. Etheridge, C. Trudinger, P. Steele, R. Langenfelds, T. van Ommen, A. Smith, and J. Elkins, 2006: Law dome CO_2, CH_4 and N_2O ice core records extended to 2000 years BP. *Geophys. Res. Lett.*, **33**, L14810, https://doi.org/10.1029/2006GL026152.

Mann, M. E., and Coauthors, 2009: Global signatures and dynamical origins of the Little Ice Age and Medieval Climate Anomaly. *Science*, **326**, 1256–1260, https://doi.org/10.1126/science.1177303.

——, B. A. Steinman, D. J. Brouillette, and S. K. Miller, 2021: Multidecadal climate oscillations during the past millennium driven by volcanic forcing. *Science*, **371**, 1014–1019, https://doi.org/10.1126/science.abc5810.

Ménégoz, M., C. Cassou, D. Swingedouw, Y. Ruprich-Robert, P. A. Bretonnière, and F. Doblas-Reyes, 2018: Role of the Atlantic multidecadal variability in modulating the climate response to a Pinatubo-like volcanic eruption. *Climate Dyn.*, **51**, 1863–1883, https://doi.org/10.1007/s00382-017-3986-1.

Miller, G. H., and Coauthors, 2012: Abrupt onset of the Little Ice Age triggered by volcanism and sustained by sea-ice/ocean feedbacks. *Geophys. Res. Lett.*, **39**, L02708, https://doi.org/10.1029/2011GL050168.

Moreno-Chamarro, E., D. Zanchettin, K. Lohmann, and J. H. Jungclaus, 2017: An abrupt weakening of the subpolar gyre as trigger of Little Ice Age-type episodes. *Climate Dyn.*, **48**, 727–744, https://doi.org/10.1007/s00382-016-3106-7.

Ning, L., J. Liu, and W. Sun, 2017: Influences of volcano eruptions on Asian summer monsoon over the last 110 years. *Sci. Rep.*, **7**, 42626, https://doi.org/10.1038/srep42626.

Otterå, O. H., M. Bentsen, H. Drange, and L. Suo, 2010: External forcing as a metronome for Atlantic multidecadal variability. *Nat. Geosci.*, **3**, 688–694, https://doi.org/10.1038/ngeo955.

Otto-Bliesner, B. L., and Coauthors, 2016: Climate variability and change since 850 CE: An ensemble approach with the Community Earth System Model. *Bull. Amer. Meteor. Soc.*, **97**, 735–754, https://doi.org/10.1175/BAMS-D-14-00233.1.

PAGES 2k Consortium, 2013: Continental-scale temperature variability during the past two millennia. *Nat. Geosci.*, **6**, 339–346, https://doi.org/10.1038/ngeo1797.

Rayner, N. A., D. E. Parker, E. B. Horton, C. K. Folland, L. V. Alexander, D. P. Rowell, E. C. Kent, and A. Kaplan, 2003: Global analyses of sea surface temperature, sea ice, and night marine air temperature since the late nineteenth century. *J. Geophys. Res.*, **108**, 4407, https://doi.org/10.1029/2002JD002670.

Richter, T. O., F. J. C. Peeters, and T. C. E. van Weering, 2009: Late Holocene (0–2.4ka BP) surface water temperature and salinity variability, Feni Drift, NE Atlantic Ocean. *Quat. Sci. Rev.*, **28**, 1941–1955, https://doi.org/10.1016/j.quascirev.2009.04.008.

Robock, A., 2000: Volcanic eruptions and climate. *Rev. Geophys.*, **38**, 191–219, https://doi.org/10.1029/1998RG000054.

Rosenbloom, N. A., B. L. Otto-Bliesner, E. C. Brady, and P. J. Lawrence, 2013: Simulating the mid-Pliocene warm period with the CCSM4 model. *Geosci. Model Dev.*, **6**, 549–561, https://doi.org/10.5194/gmd-6-549-2013.

Ruiz-Barradas, A., S. Nigam, and A. Kavvada, 2013: The Atlantic multidecadal oscillation in twentieth century climate simulations: Uneven progress from CMIP3 to CMIP5. *Climate Dyn.*, **41**, 3301–3315, https://doi.org/10.1007/s00382-013-1810-0.

Sachs, J. P., 2007: Cooling of northwest Atlantic slope waters during the Holocene. *Geophys. Res. Lett.*, **34**, L03609, https://doi.org/10.1029/2006GL028495.

Schleussner, C. F., and G. Feulner, 2013: A volcanically triggered regime shift in the subpolar North Atlantic Ocean as a possible origin of the Little Ice Age. *Climate Past*, **9**, 1321–1330, https://doi.org/10.5194/cp-9-1321-2013.

Shapiro, A. I., W. Schmutz, E. Rozanov, M. Schoell, M. Haberreiter, A. V. Shapiro, and S. Nyeki, 2011: A new approach to the long-term reconstruction of the solar irradiance leads to large historical solar forcing. *Astron. Astrophys.*, **529**, A67, https://doi.org/10.1051/0004-6361/201016173.

Sicre, M.-A., I. R. Hall, J. Mignot, M. Khodri, U. Ezat, M.-X. Truong, J. Eiríksson, and K.-L. Knudsen, 2011: Sea surface temperature variability in the subpolar Atlantic over the last two millennia. *Paleoceanogr. Paleoclimatol.*, **26**, PA4218, https://doi.org/10.1029/2011PA002169.

Sigl, M., and Coauthors, 2015: Timing and climate forcing of volcanic eruptions for the past 2,500 years. *Nature*, **523**, 543–549, https://doi.org/10.1038/nature14565.

Slawinska, J., and A. Robock, 2018: Impact of volcanic eruptions on decadal to centennial fluctuations of Arctic sea ice extent during the last millennium and on initiation of the Little Ice Age. *J. Climate*, **31**, 2145–2167, https://doi.org/10.1175/JCLI-D-16-0498.1.

Steiger, N., J. E. Smerdon, E. R. Cook, and B. I. Cook, 2018: A reconstruction of global hydroclimate and dynamical variables over the Common Era. *Sci. Data*, **5**, 180086, https://doi.org/10.1038/sdata.2018.86.

Stevenson, S., and Coauthors, 2018: Climate variability, volcanic forcing, and last millennium hydroclimate extremes. *J. Climate*, **31**, 4309–4327, https://doi.org/10.1175/JCLI-D-17-0407.1.

Sun, W., J. Liu, and Z. Wang, 2017: Simulation of centennial-scale drought events over eastern China during the past 1500 years.

J. Meteor. Res., **31**, 17–27, https://doi.org/10.1007/s13351-017-6090-x.

——, ——, B. Wang, D. Cheng, F. Liu, Z. Wang, L. Ning, and M. Chen, 2019a: A "La Niña-like" state occurring in the second year after large tropical volcanic eruptions during the past 1500 years. *Climate Dyn.*, **52**, 7495–7509, https://doi.org/10.1007/s00382-018-4163-x.

——, B. Wang, J. Liu, D. Chen, C. Gao, L. Ning, and L. Chen, 2019b: How northern high-latitude volcanic eruptions in different seasons affect ENSO. *J. Climate*, **32**, 3245–3262, https://doi.org/10.1175/JCLI-D-18-0290.1.

——, J. Liu, B. Wang, D. L. Chen, and C. C. Gao, 2022: Pacific multidecadal (50–70 year) variability instigated by volcanic forcing during the Little Ice Age (1250–1850). *Climate Dyn.*, **59**, 231–244, https://doi.org/10.1007/s00382-021-06127-7.

Sutton, R. T., and D. L. R. Hodson, 2005: Atlantic Ocean forcing of North American and European summer climate. *Science*, **309**, 115–118, https://doi.org/10.1126/science.1109496.

Swingedouw, D., J. Mignot, P. Ortega, M. Khodri, M. Menegoz, C. Cassou, and V. Hanquiez, 2017: Impact of explosive volcanic eruptions on the main climate variability modes. *Global Planet. Change*, **150**, 24–45, https://doi.org/10.1016/j.gloplacha.2017.01.006.

Tardif, R., and Coauthors, 2019: Last millennium reanalysis with an expanded proxy database and seasonal proxy modeling. *Climate Past*, **15**, 1251–1273, https://doi.org/10.5194/cp-15-1251-2019.

Thiéblemont, R., K. Matthes, N. E. Omrani, K. Kodera, and F. Hansen, 2015: Solar forcing synchronizes decadal North Atlantic climate variability. *Nat. Commun.*, **6**, 8268, https://doi.org/10.1038/ncomms9268.

Thornalley, D. J. R., H. Elderfield, and I. N. McCave, 2009: Holocene oscillations in temperature and salinity of the surface subpolar North Atlantic. *Nature*, **457**, 711–714, https://doi.org/10.1038/nature07717.

Ting, M., Y. Kushnir, R. Seager, and C. Li, 2009: Forced and internal twentieth-century SST trends in the North Atlantic. *J. Climate*, **22**, 1469–1481, https://doi.org/10.1175/2008JCLI2561.1.

Trenberth, K. E., and D. J. Shea, 2006: Atlantic hurricanes and natural variability in 2005. *Geophys. Res. Lett.*, **33**, L12704, https://doi.org/10.1029/2006GL026894.

Wang, J., B. Yang, F. C. Ljungqvist, J. Luterbacher, T. J. Osborn, K. R. Briffa, and E. Zorita, 2017: Internal and external forcing of multidecadal Atlantic climate variability over the past 1,200 years. *Nat. Geosci.*, **10**, 512–517, https://doi.org/10.1038/ngeo2962.

Wang, Q., R. Ricker, and L. Mu, 2021: Arctic sea ice decline preconditions events of anomalously low sea ice volume export through Fram Strait in the early 21st century. *J. Geophys. Res. Oceans*, **126**, e2020JC016607, https://doi.org/10.1029/2020JC016607.

Wang, Z., Y. Li, B. Liu, and J. Liu, 2015: Global climate internal variability in a 2000-year control simulation with Community Earth System Model (CESM). *Chin. Geogr. Sci.*, **25**, 263–273, https://doi.org/10.1007/s11769-015-0754-1.

Yang, H., and Q. Wen, 2020: Investigating the role of the Tibetan Plateau in the formation of Atlantic meridional overturning circulation. *J. Climate*, **33**, 3585–3601, https://doi.org/10.1175/JCLI-D-19-0205.1.

Zhong, Y., G. H. Miller, B. L. Otto-Bliesner, M. M. Holland, D. A. Bailey, D. P. Schneider, and A. Geirsdottir, 2011: Centennial-scale climate change from decadally-paced explosive volcanism: A coupled sea ice–ocean mechanism. *Climate Dyn.*, **37**, 2373–2387, https://doi.org/10.1007/s00382-010-0967-z.